

1 **Title:** A novel approach to partitioning evapotranspiration into evaporation and transpiration
2 in flooded ecosystems

3

4 **Running Title:** A novel approach to T/ET partitioning

5

6 **Authors:** Elke Eichelmann^{*a}, Mauricio C. Mantoani^a, Samuel D. Chamberlain^b, Kyle S.
7 Hemes^b, Patricia Y. Oikawa^c, Daphne Szutu^b, Alex Valach^{b^}, Joseph Verfaillie^b, and Dennis
8 D. Baldocchi^b

9

10 **Affiliation:**

11 ^a School of Biology and Environmental Science, University College Dublin, Science Centre
12 West, Belfield, Dublin 4, Ireland

13 ^b Department of Environmental Science, Policy & Management, UC Berkeley, 130 Mulford
14 Hall, Berkeley, CA, 94720, USA

15 ^c Department of Earth and Environmental Sciences, California State University, East Bay,
16 North Science room 329, Hayward, CA, 94542, USA

17 [^] now at: Climate and Agriculture Group, Agroscope, 191 Reckenholzstrasse, 8046 Zurich,
18 Switzerland

19

20 ^{*}Corresponding author; tel. +353 (0)1 716 2020; Elke.Eichelmann@ucd.ie

21

22

24

25 **Abstract:** Reliable partitioning of micrometeorologically measured evapotranspiration (ET)
26 into evaporation (E) and transpiration (T) would greatly enhance our understanding of the
27 water cycle and its response to climate change. While some methods on ET partitioning have
28 been developed, their underlying assumptions make them difficult to apply more generally,
29 especially in sites with large contributions of E. Here, we report a novel ET partitioning
30 method using Artificial Neural Networks (ANN) in combination with a range of
31 environmental input variables to predict daytime E from nighttime ET measurements. The
32 study uses eddy covariance data from four restored wetlands in the Sacramento-San Joaquin
33 Delta, California, USA, as well as leaf-level T data for validation. The four wetlands vary in
34 structure from some with large areas of open water and little vegetation to very densely
35 vegetated wetlands, representing a range of ET conditions. The ANNs were built with
36 increasing complexity by adding the input variable that resulted in the next highest average
37 value of model testing R^2 across all sites. The order of variable inclusion (and importance)
38 was: vapor pressure deficit (VPD) > gap-filled sensible heat flux (H_{gf}) > air temperature
39 (T_{air}) > friction velocity (u_*) > other variables. Overall, 36 ANNs were analyzed. The model
40 using VPD, H_{gf} , T_{air} , and u_* (F11), showed an average testing R^2 value across all sites of
41 0.853. In comparison with the model that included all 10 variables (F36), F11 generally
42 performed better during validation with independent data. In comparison to other methods
43 described in the literature, the ANN method generated more consistent T/ET partitioning
44 results especially for more complex sites with large E contributions. Our method improves
45 the understanding of T/ET partitioning. While it may be particularly suited to flooded
46 ecosystems, it can also improve T/ET partitioning in other systems, increasing our knowledge
47 of the global water cycle.

48

49 **Key-words:** artificial neural networks; eddy covariance; machine learning; latent energy;
50 terrestrial water cycle; wetlands; vapor pressure deficit.

51 **1 Introduction:**¹

52

53 Evapotranspiration² (ET) is the combined water loss from terrestrial ecosystems via
54 transpiration (T), i.e., water lost by plants during the process of carbon assimilation, and
55 evaporation (E), i.e., water lost via direct evaporation of soil and surface water. Through
56 these processes, ET adds on the order of 65 to 75 thousand km³ of water to the atmosphere
57 every year (Oki & Kanae, 2006; Trenberth, Fasullo, & Kiehl, 2009; Jung et al., 2018) and
58 constitutes an important component of the terrestrial water cycle. Despite its importance to
59 the global water cycle, ET is currently poorly constrained in global land surface models
60 (LSM), and it is unclear whether ET will increase or decrease with climate change which
61 creates large uncertainties in climate predictions (Brutsaert & Parlange, 1998; Zeng et al.,
62 2018). This is partly because E and T have different drivers and mechanisms. Thus,
63 improving our understanding of the relative contribution of E and T to ET will improve our
64 ability to predict how the water cycle will evolve with climate change (Stoy et al., 2019).

65 Assessments of E and T fluxes at an ecosystem scale (i.e., 100 m to km) have been
66 attempted using a variety of methods (Stoy et al., 2019). While some methods attempt to
67 determine E and T components by direct measurements (e.g., measurement of soil
68 evaporation, sap-flux measurements for transpiration), these are often time and labor
69 intensive and present significant challenges upscaling results to ecosystem level (Wilson et
70 al., 2001). Micrometeorological methods, such as eddy covariance (EC), are well-established
71 methods that assess biosphere-atmosphere fluxes of trace gases at the ecosystem scale
72 (Baldocchi et al., 1988). With EC (see Fluxnet.org, 2021) continuous measurements of

1 1 Abbreviations: ANN = Artificial Neural Networks; EC = Eddy Covariance; E = evaporation; ET =
2 evapotranspiration; GCC = vegetation greenness index; GEP = Gross Ecosystem Productivity; T = transpiration;
3 WT = water table; WUE = Water Use Efficiency; VPD = vapor pressure deficit;

4 2 NB: There is some discussion in the community around the correct use of the terms
5 evapotranspiration vs evaporation (Miralles et al, 2020). We have opted to follow the common use of the term
6 evapotranspiration throughout this manuscript to describe the total biosphere-atmosphere water flux,
7 including transpiration as well as direct evaporation from soil and surface waters.

73 ecosystem trace gas fluxes such as water vapor can be made on time scales from individual
74 half hours to years (Baldocchi, 2003). However, it can generally only provide direct
75 measurements of the net biosphere-atmosphere flux above the plant canopy. In the case of
76 water vapor fluxes, this includes the net flux of E and T combined. The ability to partition
77 micrometeorologically measured ET fluxes into E and T components would greatly improve
78 our understanding of the pathways by which ecosystems use water, including how E and T
79 components change on different timescales and with changing climatic conditions, as well as
80 the impact of site-specific characteristics like vegetation cover heterogeneity (Eichelmann et
81 al., 2018).

82 While there are several well tested and established methods to partition net
83 ecosystem CO₂ fluxes into its components of gross primary production and ecosystem
84 respiration (Baldocchi, 2003; Reichstein et al., 2005; Desai et al., 2008), less work has been
85 done on partitioning ET fluxes (Stoy et al., 2019). Stoy et al. (2019) provide a review of the
86 most common methods for determining E and T fluxes at ecosystem level. Most methods
87 proposed for partitioning micrometeorologically measured ET fluxes use the intrinsic
88 relationship between CO₂ uptake and transpirational water loss, linked through stomatal
89 exchange at the plant level, to estimate ecosystem T (e.g., Scanlon and Sahu, 2008; Zhou et
90 al., 2016; Scott and Biederman, 2017; Nelson et al., 2018; Li et al., 2019). Scott and
91 Biederman (2017) proposed a method to partition long-term ET measurements into E and T.
92 Their method provides multi-year averages of partitioning on a weekly to yearly timescale.
93 However, it requires datasets of multiple year lengths with high interannual consistency in
94 seasonal ecosystem ET behavior. Furthermore, it is unclear if this method provides reliable
95 results in systems that have a large contribution of E or large interannual variation in
96 ecosystem water exchange behavior.

97 Similarly, the partitioning method proposed by Scanlon and Sahu (2008), Scanlon
98 and Kustas (2010), and Skaggs et al. (2018), uses the correlation between the high frequency

99 fluctuation of water vapor and CO₂ concentrations to determine the stomatal and non-
100 stomatal mediated components of the net water and CO₂ fluxes. However, this method relies
101 on the knowledge of water use efficiency (WUE), which is the ratio of carbon uptake through
102 photosynthesis to water loss through T, at the plant or leaf-level. Since information on WUE
103 is not always readily available at the temporal scale required for this method, and because
104 WUE can change over time with successional age and environmental factors like CO₂
105 fertilization, it restricts the wider use of this method. Another method based on the
106 relationship between CO₂ uptake and T proposed by Zhou et al. (2016) to partition ET data
107 from EC measurements works with the underlying assumption that there will be periods for
108 which E is zero and T/ET approaches one. Similarly, the method proposed by Nelson et al.
109 (2018) assumes that the ecosystem will be dominated by T for some time periods. While such
110 methods are an advancement on T/ET partitioning, there is space for other new approaches
111 particularly if they do not need specialized data or costly equipment to increase the wider use
112 and applicability of such techniques.

113 Ecosystems with large contributions of E, where total ET is not always dominated
114 by T and which have complex interrelationships between ecosystem productivity, E, and T,
115 might violate some or all of the underlying assumptions necessary for partitioning methods
116 based on the relationship between CO₂ uptake and water loss to work (Stoy et al., 2019). This
117 is the case for wetlands, where the contribution of E-T is altered significantly by structural
118 factors such as areas of open water, as well as environmental factors, for instance, diurnal
119 fluctuations in air or water temperature and water table (Drexler et al., 2004; Goulden et al.,
120 2007; Eichelmann et al., 2018). In addition, the before-mentioned methods only work when
121 the ecosystem CO₂ flux is known in conjunction with ET. Although this is often the case for
122 EC measurements, there are other micrometeorological methods that provide measurements
123 of ET without measuring CO₂ fluxes. Consequently, a partitioning method that does not rely

124 on knowledge of CO₂ flux and assumptions of carbon-water flux correlations would greatly
125 enhance our ability to partition T/ET in a diversity of settings.

126 Methods applied to partition CO₂ fluxes usually use relationships of environmental
127 drivers with the individual flux components determined from time periods where only one
128 flux component is present and extrapolate these to the other periods (Reichstein et al., 2005;
129 Desai et al., 2008). Many methods (e.g., Barr et al., 2004; Reichstein et al., 2005) use
130 relationships between temperature and ecosystem respiration based on nighttime fluxes, when
131 CO₂ uptake is zero, and extrapolate these to calculate daytime ecosystem respiration. The
132 gross CO₂ uptake component is then determined as the difference between the net flux and
133 the estimated daytime ecosystem respiration. While this method works well for carbon flux
134 partitioning, where the primary driver of ecosystem respiration is considered to be
135 temperature, it can face limitations in the case of water fluxes where nighttime fluxes are
136 often very small and the drivers of E and T are complex. However, it has been shown that
137 nighttime T from plants is usually very small in many ecosystems (Caird et al., 2006;
138 Dawson et al., 2007). Thus, for non-water limited systems with large contributions of E, such
139 as wetlands, we can approximate nighttime water fluxes as exclusively E.

140 A newer approach used to partition net ecosystem carbon fluxes into the individual
141 components of gross primary production and ecosystem respiration uses Artificial Neural
142 Networks (ANN) (Papale & Valentini, 2003; Desai et al., 2008; Tramontana et al., 2020).
143 Although the use of ANNs could also be directed at T/ET partitioning, the application of this
144 technique has not been done yet and needs further exploration. Since machine learning
145 methods can resolve complex, nonlinear relationships between environmental drivers and
146 flux variables (Tramontana et al., 2020), ANNs are a promising approach to partition T/ET in
147 ecosystems where existing ET partitioning methods face limitations, such as wetlands and
148 river deltas.

149 The Sacramento-San Joaquin River Delta (hereafter, the Delta) plays an essential
150 role in the water supply of the state of California, USA. The Delta supplies the majority of
151 freshwater to large metropolises in Southern California and provides water for irrigation of
152 crops in the Central Valley (Deverel & Rojstaczer, 1996). Historically, the Delta's peat soils
153 were flooded with large areas of freshwater marsh, but the majority of the Delta land area is
154 now actively drained and cultivated for agriculture. More recently, however, there has been a
155 growing interest in restoring freshwater wetlands to prevent further soil subsidence. In one of
156 the approaches used, the restored wetlands in the Delta are flooded with a water table that is
157 above ground level at all times (Hemes et al., 2019). The four restored wetlands in the Delta
158 selected for this study represent a range of conditions with some sites dominated by open
159 water areas and others covered in dense vegetation throughout (Eichelmann et al., 2018),
160 representing varying amounts of T/ET ratios expected at the different sites.

161 While restoring freshwater wetlands in the Delta can have many benefits, including
162 those related to wildlife habitat, climate, recreation, and levee stability, it can also lead to
163 increased water loss through ET depending on the vegetation cover characteristics
164 (Eichelmann et al., 2018). Moreover, given that changes in local and regional ET can affect
165 cloud formation and precipitation distribution (Gerken et al., 2018), this may have a knock-on
166 effect on the water cycle and on the climate feedback of wetlands (Hemes et al., 2018). In
167 locations that experience spatial and temporal water shortages, such as California, increasing
168 our knowledge of the local water cycle and understanding how ET is affected by external
169 drivers is extremely important.

170 Here, we show that we can partition ET measurements above flooded wetlands in
171 the Delta by predicting daytime E from nighttime ET measurements using ANNs in
172 combination with environmental driver variables such as vapor pressure deficit (VPD),
173 temperature, atmospheric turbulence, canopy greenness index, and others. The meso-network
174 of diverse wetland EC sites used in this study is ideal to test this new ET partitioning method

175 as it provides a continuum of T/ET conditions across complex canopy architectures. We
176 present the most promising models and discuss the application of ANN to partition T/ET
177 measurements. While there is an emphasis on wetlands, we show evidence that our method
178 may be applied to other ecosystems as well, increasing the knowledge of the water cycle and
179 shedding light on plant-water productivity relationships at an ecosystem level.

180

181 **2 Methods**

182

183 **2.1 Site Description**

184

185 We conducted EC measurements at four wetland sites in the Sacramento-San
186 Joaquin river delta in Northern California: West Pond (38° 6.44'N, 121° 38.81'W, Ameriflux
187 ID: US-TW1), East End (38° 6.17'N, 121° 38.48'W, Ameriflux ID: US-TW4), Mayberry
188 Farms (38° 2.99'N, 121° 45.90'W, Ameriflux ID: US-MYB), and Sherman Island (38° 2.21'N
189 121° 45.28'W, Ameriflux ID: US-Sne). All sites are part of the Ameriflux network and the
190 EC data from these sites are available for download through the Ameriflux data sharing
191 platform (<https://ameriflux.lbl.gov/>). The sites have been described in detail in other
192 publications (Detto et al., 2010; Hatala et al., 2012; Knox et al., 2015; Eichelmann et al.,
193 2018; Hemes et al., 2018, 2019) and their main characteristics will only be briefly
194 summarized here. All four wetlands are artificially constructed wetlands managed by the
195 Department of Water Resources to reverse soil subsidence in the area. The water table is
196 actively managed to be above ground level throughout the flooded portions of the wetlands at
197 all sites.

198 The West Pond wetland is the oldest of the four wetlands, originally constructed in
199 1998. It is the most homogeneous of the study sites, with a fairly even, but slightly sloping,
200 ground surface and dense vegetation covering the whole wetland (97% vegetation cover

201 within EC footprint in 2018, Valach et al., 2021). The water table varies slightly throughout
202 the wetland due to the sloping ground level but is generally between 20 and 40 cm above
203 ground level. The Mayberry Farms wetland was constructed in 2010 and has a very
204 heterogeneous footprint. With a heterogeneous bathymetry this wetland features small islands
205 of vegetation and deeper channels and pools of open water (64% vegetation cover within EC
206 footprint in 2018, Valach et al., 2021). The water depth varies from 2 m above ground level
207 to 2 cm above ground level in the flooded portions, with some dry areas. The East End
208 wetland was constructed in 2013 and also features some areas of open water channels and
209 pools. The vegetation at East End has filled in more evenly since its establishment and it has
210 a greater vegetation cover than Mayberry Farms (96% vegetation cover within EC footprint
211 in 2018, Valach et al., 2021). The Sherman Island wetland is the newest wetland constructed
212 in 2016. Similarly to Mayberry Farms, it features a very heterogeneous bathymetry and the
213 footprint is dominated by large portions of open water. Vegetation has only taken hold in
214 very few and small patches within the footprint of the EC measurements (45% vegetation
215 cover within EC footprint in 2018, Valach et al., 2021). While the individual make-up and
216 proportions vary slightly between sites, the dominant vegetation species at all sites are tules
217 (*Schoenoplectus acutus*) and cattails (*Typha* spp.) (O'Connell et al., 2015).

218

219 **2.2 Eddy Covariance Data**

220

221 We measured continuous fluxes of H₂O, CO₂ and sensible heat using the EC method
222 at all sites (Baldocchi et al., 1988). A detailed description of the instrument set-up and
223 calculation procedures can be found in previously published papers (Detto et al., 2010; Hatala
224 et al., 2012; Knox et al., 2015; Eichelmann et al., 2018; Hemes et al., 2018, 2019) and will
225 only be summarized here. At each site, the EC instrumentation consisted of a sonic
226 anemometer (WindMaster 1590 or WindMaster Pro 1352, Gill Instruments Ltd, Lymington,

227 Hampshire, England) and an open path trace gas analyzer for H₂O and CO₂ concentrations
228 (LI-7500 or LI-7500A, LI-COR Inc., Lincoln, NE, USA). The instruments were mounted at a
229 fixed height at least 1 m above the maximum height of the canopy.

230 High frequency (20 Hz) measurements of sonic temperature, three-dimensional wind
231 speed, and trace gas concentrations were recorded on USB drives in the field through the
232 analyzer interface (LI-7550, LI-COR Inc., Lincoln, NE, USA). The data were collected
233 approximately every two weeks, with routine maintenance and servicing of the instruments
234 taking place at the same time. The LI-7500 trace gas analyzers were calibrated approximately
235 every three to six months in the laboratory. The performance of the EC set-up was also cross
236 checked periodically at individual sites by the Ameriflux mobile EC reference system
237 (Schmidt et al., 2012).

238 All data processing and filtering was performed offline. Thirty-minute average
239 fluxes were calculated using custom software written in-house (MATLAB, MathWorks Inc.,
240 R2015b, version 8.6.0) after basic de-spiking of high frequency data and filtering for
241 instrument malfunctioning (Detto et al., 2010; Hatala et al., 2012; Knox et al., 2015;
242 Eichelmann et al., 2018). A rotation into the mean wind was performed for each 30-minute
243 averaging interval and the Webb-Pearman-Leuning correction for air density fluctuations for
244 open path sensors was applied to the calculated fluxes (Webb et al., 1980). Fluxes were
245 filtered for low friction velocity (u_*), as well as based on stability and turbulence conditions
246 (Foken & Wichura, 1996). Low friction velocity thresholds are based on the point where
247 nighttime CO₂ fluxes become independent of u_* and are defined individually at each site. The
248 thresholds can vary seasonally and usually range from 0.12 m s⁻¹ to 0.2 m s⁻¹. Because of the
249 narrow shape of the wetland, the West Pond wetland fluxes were also filtered by wind
250 direction to ensure flux footprints originated from the ecosystem of interest.

251 Energy budget closure is often used as a quality indicator for EC data (Wilson et al.,
252 2002). At the flooded wetland sites covered in this study the energy budget closure of daily

253 totals was between 73% and 81%, which is slightly lower than typically found in dry
254 ecosystems. H₂O fluxes from the West Pond, Mayberry Farms, and East End wetland sites
255 used in this study have been published and discussed in detail by Eichelmann et al. (2018),
256 including a discussion of data quality, energy budget closure, and the difficulties estimating
257 energy storage components in the flooded wetlands. Because of the importance of storage
258 terms in the context of these sites, energy fluxes measured by the EC method have not been
259 adjusted for incomplete energy budget closure (Eichelmann et al., 2018). In this study,
260 positive fluxes indicate a gain to the atmosphere and negative fluxes indicate a loss from the
261 atmosphere. All analyzes and data processing described in this study were performed using
262 MATLAB (MathWorks Inc., R2018a, version 9.4.0).

263

264 **2.3 Auxiliary Data**

265

266 Meteorological and environmental data were also measured continuously in addition
267 to EC data at all sites. The following auxiliary measurements were available at all wetland
268 sites: Air temperature (T_{air}); water temperature at 3 to 6 different water depths (T_{water} , depths
269 vary between site due to differences in water tables); soil temperature at 6 different depths
270 (T_{soil}); relative humidity (RH); atmospheric pressure; incoming and outgoing shortwave
271 radiation; incoming and outgoing longwave radiation; net radiation; incoming and outgoing
272 photosynthetically active radiation; water table depth; water conductivity; and vegetation
273 greenness index from camera data (GCC). Moreover, the West Pond and East End wetland
274 sites were equipped with a rain gauge to measure precipitation and the East End wetland site
275 was equipped to measure ground heat flux (G).

276 Data were recorded as half hour averages (or totals in the case of precipitation) with
277 individual sampling frequency varying between 1 and 15 minutes depending on the sensor.
278 Specifically of interest for this study are measurements of vapor pressure deficit (VPD),

279 water table depth (WT), air temperature (T_{air}), vegetation greenness index (green chromatic
280 coordinate; GCC), and net radiation (R_{net}). VPD was calculated from relative humidity
281 measurements in combination with air temperature data, both measured with aspirated and
282 wind-shielded humidity and temperature probes (HMP-60, Vaisala Inc., Helsinki, Finland).
283 Net radiation was measured using either a net radiometer (NR-LITE Radiometer, Hukseflux,
284 Delft, the Netherlands; at Mayberry Farms) or a four-component net radiometer (NR01 Net
285 Radiometer, Hukseflux, Delft, the Netherlands; at West Pond, East End, and Sherman
286 Island).

287

288 **2.4 Artificial Neural Network Partitioning Routine**

289

290 Artificial Neural Networks have been applied for gap-filling and partitioning EC
291 fluxes in the past (Papale & Valentini, 2003; Oikawa et al., 2017; Tramontana et al., 2020).
292 Specifically, for CO_2 fluxes, ANNs have shown to perform well when used to gap-fill
293 missing data (Moffat et al., 2007) and partitioning net CO_2 fluxes into the component fluxes
294 of gross primary production (GPP) and ecosystem respiration (R_{eco}) (Desai et al., 2008;
295 Oikawa et al., 2017; Tramontana et al., 2020). Following a similar approach to partitioning
296 CO_2 data, we assumed that nighttime ET data is dominated by E at these flooded sites:

297

$$298 \quad ET = T + E \quad (1)$$

$$299 \quad T_{\text{night}} \cong 0 \quad (2)$$

$$300 \quad ET_{\text{night}} = E \quad (3)$$

301

302 We conducted several leaf-level chamber measurements using a LI-6400 Portable
303 Photosynthesis System (LI-COR Inc., Lincoln, NE, USA) throughout the growing season of

304 2017 to confirm that nighttime and dark T flux is indeed negligible at these sites. The
305 available nighttime E data is used in combination with environmental input variables to train
306 the ANN routine to predict daytime E. Daytime T was then calculated as the difference
307 between total ET and E:

308

$$309 \quad T_{day} = ET_{measured} - E_{predicted} \quad (4)$$

310 Before ET partitioning was performed all flux data were gap-filled using ANN routines
311 described in previous studies (Knox et al., 2015, 2016; Oikawa et al., 2017, Eichelmann et
312 al., 2018).

313

314 **2.4.1 Artificial Neural Network Routine Set-up**

315

316 To partition ET data using ANNs in this study, we followed a similar set-up and
317 architecture as described for gap-filling and partitioning CO₂ data in previous studies
318 (Balocchi & Sturtevant, 2015; Knox et al., 2015, 2016; Oikawa et al., 2017). The entire
319 available (multi-year) explanatory dataset was split into 20 data clusters using the k-means
320 clustering algorithm. The data used for training, testing, and validation of the ANNs was
321 proportionally sampled from these clusters with one third of the available data used for
322 training, testing, and validation each. This procedure avoids a sampling bias towards periods
323 when more data are available, such as a specific time of the year or time of the day.
324 Proportional data sampling from the k-means clusters into training, testing, and validation
325 data was repeated 20 times. For each of the 20 re-sampled training, testing, and validation
326 datasets several ANN architectures were tested starting with one hidden layer and the same
327 number of nodes as the number of explanatory input variables ($n_{inputvar}$). Each architecture was
328 initialized 10 times with random starting weights and the initialization with the lowest mean
329 sampling error was used. The complexity of the ANN architecture was increased first by

330 increasing the number of nodes to 1.5 times n_{inputvar} and then by increasing the number of
331 hidden layers until a further increase in complexity results in less than 5% reduction of the
332 mean standard error. For our datasets, this commonly resulted in the use of an architecture
333 with two hidden layers, the first one with n_{inputvar} nodes, the second one with $0.5 * n_{\text{inputvar}}$ nodes,
334 although for some sites and input variable combinations architectures with only one hidden
335 layer produced better results. The ‘validation’ step within the ANN procedure described
336 above is performed on nighttime data only and is therefore distinctly different from the
337 validation with flooding and leaf level data described below. Throughout the remainder of the
338 manuscript when we use the term ‘validation’ we refer to the independent flooding and leaf
339 level data validation. The ANN internal validation routine based on nighttime data is referred
340 to as ‘testing’.

341

342 **2.4.2 Selection of Explanatory Variables**

343

344 A number of different explanatory environmental input variables were tested
345 individually and in combination. Based on the general understanding of the drivers of E
346 fluxes in terrestrial and aquatic ecosystems we tested the following input parameters:
347 Meteorological and environmental variables: VPD, R_{net} , GCC, WT, T_{air} ; Flux variables:
348 friction velocity (u_*), gap-filled sensible heat flux (H_{gf}), gap-filled CO_2 flux (wc_{gf}), and
349 ecosystem respiration ($er_{\text{Reichstein}}$) partitioned using the temperature dependency method
350 proposed by Reichstein et al. (2005). In addition, we used a running decimal timestamp
351 (datetime) as input variable in all our ANN runs. VPD, u_* , and T_{air} describe the atmospheric
352 demand driving E. R_{net} and H_{gf} are connected to ET (or latent energy) through the energy
353 balance equation. GCC, wc_{gf} , and $er_{\text{Reichstein}}$ are directly or indirectly related to plant
354 physiological responses that can impact ET components. Finally, WT is related to the water
355 budget of the ecosystem. Given the strong correlation of water temperature (T_{water}) with

356 nighttime ET documented at these sites in a previous study (Eichelmann et al., 2018) we
357 would also expect T_{water} to perform well as an environmental input variable. Unfortunately,
358 we were unable to include T_{water} as an input variable in this study since we did not have
359 consistent T_{water} measurements across time for any of the four sites.

360 We ran the ANN routine for each of these parameters individually and recorded the
361 R^2 value and slope of the linear regression of the nighttime EC data initially set aside for
362 testing within the ANN routine versus the predictions. This R^2 value is called ‘testing R^2 ’
363 throughout this manuscript and is based only on nighttime data. Starting with the input
364 parameter with the highest testing R^2 , we ran the ANN routine with increasing numbers of
365 input variables, each time adding on the variable with the next highest testing R^2 value. We
366 continued this process until a further increase in input variables resulted in less than 1%
367 increase in the testing R^2 value. We averaged the testing R^2 values across the four sites and
368 used this value to estimate increases in the performance of the ANNs. While this average
369 testing R^2 does not have any statistical relevance, it gave us a good indicator on how well the
370 models performed across all sites studied.

371

372 **2.5 Validation of Results**

373

374 One of the main issues facing validation of ET partitioning methods is often the lack
375 of independent E or T data to validate against (Stoy et al., 2019). Taking independent
376 measurements of ecosystem E or T is challenging and one of the main reasons why
377 partitioning approaches for EC measurements of ET are much sought after. Since we do not
378 have independent measurements of ecosystem level E or T available at our sites, we reverted
379 to validating our partitioning data by a conditional sampling approach, selecting EC
380 measurement data from certain time periods when E and T can be known or closely
381 approximated to compare with the ANN predicted E or T. One of these time periods is the

382 initial time right after flooding of the wetland (referred to as flooding data), when vegetation
383 had not yet established within the footprint of our instruments. During this time, it can be
384 assumed that the entire H₂O flux coming off the surface is from E, with negligible T.

385 Since we trained our ANN routines only on nighttime data, we were able to use
386 the daytime data during the initial flooding period as an independent validation dataset for E.
387 Apart from the initial flooding period, T can also be assumed to be small to negligible during
388 the senescent winter months. However, since the plants are not harvested or otherwise
389 removed and the climate in this region is fairly mild, some do stay green throughout the
390 winter and may continue to be photosynthetically active. Additionally, vegetation on dry
391 areas such as levees usually starts to green up during the winter months in this region. Both of
392 these would be contributing to a small T flux from the ecosystem. Moreover, ET fluxes
393 during the winter period are generally lower and subject to larger errors due to more
394 challenging turbulence conditions during this time. Such conditions result in large relative
395 error in flux measurements during this period limiting the insights gained from the validation
396 during the senescent winter period. Nonetheless, we included validation of E predicted from
397 our ANN method against E measured during winter times to further test the performance of
398 our method.

399 In addition to the validation during periods when T was zero, we also conducted a
400 number of leaf-level T measurements in the summer of 2017 at the East End wetland using a
401 LI-6400 portable photosynthesis system (LI-COR Inc., Lincoln, NE, USA) with a clear
402 conifer chamber (part number 6400-05) encasing sections of the leafs or culms. Six
403 individual leaf-level measurement points (three for each of the dominant plant species) taken
404 during the same half hour period were pooled to allow comparison with the half hourly EC
405 data. These measurements provided us with an estimate of T per unit of sunlit leaf area and
406 may potentially be converted to the ecosystem scale if the ecosystem leaf area index and the
407 leaf angle distribution are known. Efforts have been made to estimate the leaf area index in a

408 number of the wetlands in the study region, however, due to the high heterogeneity and litter
409 accumulation in these systems there is a high level of uncertainty associated with the
410 measured leaf area indexes (Dronova & Taddeo, 2016). Additionally, the leaf angle
411 distribution is unknown in these systems and can only be approximated, which is an intrinsic
412 limitation of this technique.

413 Taking all these uncertainties into account, ecosystem T scaled up from leaf-level
414 measurements is associated with very large error intervals and cannot serve as a reasonable
415 constraint on the absolute values of our ANN partitioned T fluxes. However, since the scaling
416 factors to convert leaf-level values to ecosystem level are constant multipliers, we should still
417 be seeing a linear relationship between the leaf-level flux and the partitioned ecosystem level
418 T if our partitioning algorithm predicts the correct T behavior across a range of
419 environmental conditions. While we may not be able to compare the absolute T values, we
420 can compare the response cycle of ANN predicted T with the field measurements to validate
421 that we are predicting the right behavior.

422

423 **2.6 Comparison with Other T/ET Partitioning Approaches**

424

425 Direct comparisons with the Scott and Biederman's (2017) method were carried out
426 in order to evaluate the performance of our own models against their approach. For that, we
427 used the model (F11, see Results below) that achieved the best R^2 value against the validation
428 with leaf-level/flooding data. While Scott and Biederman (2017) forced all monthly
429 regressions between ET and gross ecosystem productivity (GEP) to the same slope, we used
430 different slopes for each regression. This was done to ensure the best fitting since our datasets
431 did not show the same uniform behavior across months. Indirect comparisons with other
432 methodologies mentioned above were also discussed.

433

434 **3 Results**

435

436 **3.1 Artificial Neural Network Architecture Performances**

437

438 Alongside the basic timestamp (datetime), VPD and T_{air} were the meteorological
439 variables that best explained our data when only looking at the nighttime testing data, with
440 average testing R^2 values across all sites of 0.648 and 0.565, respectively (Table 1 and
441 Supplementary Table 1). The flux related variables that showed the highest average testing R^2
442 values and added most information to the models were H_{gf} (testing R^2 of 0.620) and u_*
443 (testing R^2 of 0.531). To increase the ANNs complexity we, therefore, followed the variables
444 order of $VPD > H_{\text{gf}} > T_{\text{air}} > u_*$, adding each of them into the models sequentially. VPD was
445 the variable that contributed the most to increase the testing R^2 values of the ANNs, with an
446 average increase of 24% across all sites and a maximum of 36% for West Pond, when models
447 F21 and F26 were compared (Table 1). The incorporation of H_{gf} was responsible for an
448 average increase of 10% in testing R^2 , when comparing the ANNs F26 and F33 (Table 1). T_{air}
449 only increased the ANNs testing R^2 by 1% (i.e., when comparing models F33 and F34),
450 however, when we added u_* , the average testing R^2 value increased across all sites by 9%,
451 when comparing models F34 and F11 (Table 1). Thus, building the ANN F11 using datetime,
452 VPD, H_{gf} , T_{air} , and u_* , the average testing R^2 value across all sites reached 0.853, with a
453 minimum of 0.728 (West Pond) and a maximum of 0.910 (Sherman Island; Supplementary
454 Table 1).

455 Of all the 36 ANNs tested, the highest average testing R^2 (0.891) was reached when
456 all the explanatory variables (i.e., datetime, H_{gf} , u_* , wc_{gf} , $er_{\text{Reichstein}}$, VPD, T_{air} , GCC,
457 Rnet and WT) were put into the model F36 (Table 1 and Supplementary Table 1).
458 Consequently, on average, all the other variables analyzed (i.e., wc_{gf} , $er_{\text{Reichstein}}$, GCC,
459 Rnet and WT) accounted for less than 4% of the testing R^2 value across all the four sites

460 (when comparing models F36 and F11; Table 1). The top five ANNs (F36 > F14 > F20 > F35
461 > F11) that performed better than 0.85 all have datetime, VPD, H_{gf}, T_{air}, and u_{*} as their
462 explanatory variables and all the 11 ANNs that scored an average testing R² higher than 0.80
463 have both VPD and u_{*} in their models (Table 1 and Supplementary Table 1). Fifteen ANNs
464 showed an average testing R² higher than 0.70 and the lowest average testing R² among these
465 (0.730) was presented by the ANN F2, constructed using only datetime, T_{air}, and u_{*}
466 (Supplementary Table 1). Unsurprisingly, the lowest average testing R² (0.410) of all the 36
467 ANNs analyzed was given by the ANN built using datetime alone (F21). The slope values
468 (Table 1 and Supplementary Table 2) of the different ANNs followed quite closely the
469 pattern described for the increase in testing R² values.

470

471 **3.2 Validation of Artificial Neural Networks**

472

473 **3.2.1 Flooding Validation**

474

475 To evaluate the performance of our ANN partitioning method, we compared the
476 model predicted E with EC measurement data from conditionally sampled post-flooding
477 periods, during which we assume T to be negligible (Table 2). The ANN F11 showed the
478 highest validation R² values for East End (0.81), Mayberry Farms (0.69), and Sherman Island
479 (0.82). These values surpassed those from the model F36 (most complex), which reached
480 0.51, 0.56, and 0.53, for East End, Mayberry Farms, and Sherman Island, respectively. Figure
481 1 shows the validation comparison between F11 and F36 for the three sites.

482

483 **3.3.2 Winter Time Validation**

484

485 Judging by the observed R^2 values, the validation using daytime data from senescent
486 periods during the winter time (December to February, Table 3) performed quite poorly in
487 comparison to the validation performed with data during the initial flooding periods (Table
488 2). Nevertheless, the winter period validation overall did confirm the same trends and
489 observations as the flooding validation. At Mayberry Farms and Sherman Island ANN F11
490 again had the highest R^2 values (0.56 and 0.70, respectively). However, at East End and West
491 Pond the model F36, which included all input variables, performed best with R^2 values of
492 0.45 and 0.36, respectively. Figure 2 shows the validation comparison between F11 and F36
493 for the four sites using winter data.

494

495 **3.3.2 Validation on Diurnal Measurements of Leaf-Level Data for East End**

496

497 To evaluate the performance of our method further, we compared the model
498 predicted T with independent leaf-level data collected during a field campaign in summer
499 2017 at the East End wetland. The leaf-level data showed high variability across individual
500 measurements (Fig. 3). F11 again showed a high R^2 (0.986, Table 4). Other models (F15,
501 F33) also performed quite well in the leaf-level validation, in contrast to their performance
502 for the validation during flooding or senescent periods. The most complex ANN (F36) had a
503 lower R^2 value (0.92) for the leaf-level validation. In general, adding too many variables did
504 not lead to enhancement of validation values, but it is to be noted that all models showed a
505 high level of agreement with the leaf-level data (Table 4). Figure 3 shows both F11 and F36
506 validations against leaf-level data.

507

508

509 **3.3 Artificial Neural Networks Performance Across the Wetland Sites**

510

511 To look for model consistency across diverse canopy architecture and successional
512 stages, we compared ANN testing R^2 values between the four sites. Among the four sites,
513 East End and Sherman Island were the only sites that had ANNs with testing R^2 values larger
514 than 0.90 for the EC testing data set aside during the ANN routine (Supplementary Table 1).
515 At Sherman Island, East End, and Mayberry Farms 22, 20, and 19 ANN models reached
516 testing R^2 values above 0.70, respectively, whereas at West Pond only 11 models reached
517 testing R^2 values above 0.7 (Supplementary Table 1). In comparison with the other three
518 studied sites, West Pond showed testing R^2 values in the order of 9-18% smaller when
519 analyzing the top five ANNs with average testing R^2 larger than 0.85 (Supplementary Table
520 1). Considering all 36 ANNs, differences in testing R^2 between the same ANN for different
521 sites reached a maximum of 46%, when comparing model F6 at West Pond with Sherman
522 Island (Supplementary Table 1).

523

524 **3.4 Comparisons with Other Partitioning Approaches**

525

526 To compare our ANN method with existing T/ET partitioning methods, we applied
527 the Scott and Biederman (2017) long-term flux data partitioning method at all four sites. As
528 expected, the Scott and Biederman (2017) method worked better for datasets with > 6 years
529 (Fig. 4; Mayberry Farms, West Pond, and East End). Sherman Island, the shortest dataset
530 with four years of data collection, performed poorly, showing negative correlations of ET vs
531 GEP for the months of June to September (Fig. 4 d). Average monthly T fluxes from the
532 Scott and Biederman (2017) method for Mayberry Farms and Sherman Island (Fig. 5a and d)
533 both showed increases in T at the end of the growing season (i.e., October) out of line with
534 the observed GEP patterns. Conversely, West Pond and East End (Fig. 5b and c) showed a T
535 pattern parallel to GEP with the growing season.

536 While the T values from our ANN approach showed a similar behavior as GEP
537 during the growing season, as would be expected, the T values from the Scott and Biederman
538 (2017) method did deviate somewhat from the GEP pattern for all sites (Fig. 5). The best
539 ANN (F11) also produced more reasonable T numbers for Sherman Island compared to the
540 Scott and Biederman (2017) method. In addition, the E values retrieved in our analysis for
541 all sites were also more stable and did not fluctuate as much across months compared to the E
542 values from the Scott and Biederman (2017) method (Fig. 5). While the Scott and Biederman
543 (2017) method is not intended to produce reliable results for T/ET partitioning during winter
544 months when GEP is small, it did show very good agreement of produced E and T values
545 when compared to our ANN based values from October to February for all sites.

546

547 **3.5 Resulting Evaporation and Transpiration Estimates**

548

549 Figure 6 shows the annual (2013-2019) ANN based T/ET partitioning
550 intercomparison for all sites using ANN F11. Only years with a full year of data are used.
551 While ET stayed fairly consistent between 850-1250 mm for all sites and years (Fig. 6a),
552 GEP showed more fluctuations between the different sites, as well as interannually within
553 each site (Fig. 6b). Looking at the predicted partitioning of E and T (Fig. 6c, d), Sherman
554 Island showed the highest values of E (approximately 1100 mm) for the three years of
555 measurements available at this site, while West Pond had the lowest E values across all years
556 and sites (200 to 300 mm). Although values at East End were always higher compared to
557 Mayberry Farms for all years with measurements from both sites, decreasing pattern can be
558 observed for E at both sites, ranging from high values of 831 mm at Mayberry Farms in 2013
559 and 1119 mm at East End in 2014 down to low values of 449 mm at Mayberry and 630 mm
560 at East End in 2019. Transpiration showed opposite trends compared to E, with West Pond
561 having the highest values (between 700-800 mm in most years), followed by Mayberry Farms

562 with T values between 300-500 mm. The T pattern predicted at Mayberry Farms follows a
563 similar pattern as the GEP measurements, most notably is the significant reduction in GEP in
564 2016 which was caused by saltwater intrusion at the site (Eichelmann et al., 2018,
565 Chamberlain et al., 2020). This was mirrored in a reduction of T values in 2016, however, E
566 was not affected. Sherman Island and East End showed T values below 300 mm for all years,
567 considerably lower than the other two sites. In the first full year of measurements (2014), T at
568 East End was even predicted as negative (-24 mm), similar to the negative T predictions
569 observed at East End during the winter validation (Fig. 2). However, this value falls within
570 the uncertainty range of 91 mm for annual ET measurements at this site in 2014 (Eichelmann
571 et al., 2018). East End and Sherman Island both had a very high open water surface area,
572 especially in the first years after flooding, so it would be expected that E is more dominant.
573 Sherman Island specifically had extremely sparse vegetation cover throughout the EC
574 measurement footprint for the first two years of measurements, also evident in the very low
575 values of GEP. For both of these sites, East End and Sherman Island, we can see that
576 gradually E declines and T increases as the vegetation fills in from year to year.
577 Consequently, when comparing the T/ET values across sites (Fig. 6e), West Pond had the
578 highest value of T/ET (70%-75% on T), followed by Mayberry Farms (30%-50%), East End
579 (0-30%), and Sherman Island (<15%). This highlights that only West Pond can be described
580 as a T dominated site with T/ET values in the range between 0.5 and 0.8 reported for other
581 terrestrial ecosystems (Schlesinger & Jasechko, 2014). The other three sites are clearly E
582 dominated and have T/ET values considerably lower than those expected for terrestrial
583 ecosystems.

584

585 **4 Discussion**

586

587 **4.1 Artificial Neural Network Architecture Performances**

588

589 The ANN F36, which was built using all studied variables, presented the highest
590 average testing R^2 value (0.891) for the nighttime-based testing dataset among all 36 ANNs
591 analyzed. Nevertheless, there was not much improvement in testing R^2 in the models (i.e.,
592 maximum of 3-4% on average) after the ANN F11. This indicates that not all variables are
593 necessary to provide good results in the partitioning of ET into E and T, and that less
594 complex models can result in good predictions. For instance, using only datetime + H_{gf} +
595 VPD (F33) or datetime + u_* + T_{air} (F2) the average testing R^2 value across all sites was > 0.70 ,
596 indicating a good correlation. In addition, when using datetime + VPD alone the average
597 testing R^2 value for three sites (i.e., East End, Mayberry Farms and Sherman Island) was $>$
598 0.70.

599 In our study, the order of variable inclusion to increase model complexity was:
600 datetime $>$ VPD $>$ H_{gf} $>$ T_{air} $>$ u_* . VPD was the variable that contributed the most in the
601 improvement of the ANNs, with an average of 24% increase in testing R^2 values across all
602 sites. VPD is routinely measured at most EC sites (e.g., Fluxnet.org, 2021) and its effect on
603 ecosystem water cycling by limiting surface conductance and reducing transpiration under
604 high VPD is well documented (Buckley, 2005, Novick et al., 2016). The fact that the top 14
605 ANNs (i.e., with the highest testing R^2 value) were constructed using VPD as one of the input
606 parameters highlights the importance of VPD as a predictor of ecosystem water exchange. In
607 addition, all the 11 ANNs that scored an average testing $R^2 > 0.80$ have u_* in their models,
608 indicating that information on atmospheric turbulence is important to incorporate in ET
609 partitioning prediction if available. It may not be surprising that at these flooded sites E is
610 mainly explained by atmospheric conditions such as VPD, T_{air} , and turbulence (u_*)
611 underlining their importance in the ANN partitioning routine. At sites with different surface
612 and vegetation characteristics, such as dryland sites, it would be important to investigate the

613 importance of other variables such as soil moisture, soil temperature, or leaf wetness. It
614 would be expected that these, together with other energy balance components such as
615 radiation, would play a larger role in explaining E at water limited sites.

616

617 **4.2 Artificial Neural Network Validation Against Post-Flooding Periods and Leaf-Level**

618 **Data**

619

620 The validation of our models against data collected right after flooding (for East
621 End, Mayberry Farms, and Sherman Island) and with leaf-level data (for East End only)
622 indicated that models with less input variables (F11) performed better in comparison to the
623 model that incorporated all 10 studied variables (F36). It might be that overfitting occurred
624 when incorporating input variables that deal directly and/or indirectly with the same property/
625 factor (i.e., carbon assimilation). In this case, F36 includes $er_{Reichstein}$, wc_{gf} and GCC
626 which are all related to carbon uptake by vegetation. Thus, even with a smaller average
627 testing R^2 value, models with fewer input variables (e.g., F11) still performed better than F36
628 during validation with ground-truth leaf-level and flooding data. Specifically, the ANN F11,
629 which showed the best performance for all three of the sites with flooding data validation
630 (East End, Mayberry Farms, and Sherman Island) included $datetime + H_{gf} + VPD + T_{air} +$
631 u_* . The validation based on data collected right after flooding also emphasized the importance
632 of validating the ANN partitioning routine against data collected during daytime periods.
633 Some of the tested input variables showed strong differences in daytime and nighttime
634 behavior (e.g., R_{net}). Using these variables as inputs can lead to incorrect predictions for the
635 nighttime-based ANN routine as seen in the poor performance of F15 for the flooding
636 validation at East End and Mayberry Farms, despite a high testing R^2 of 0.75 (Supplementary
637 Table 1).

638 The flooding validation also highlights site-specific differences in the input variables
639 that provided good predictions. While the best performance was achieved with the same
640 model (F11) across all three validation sites, the behavior of the other tested models varied
641 across sites. We recommend that the selection of input parameters for ANN partitioning of
642 ET should be based on the unique site characteristics rather than a standardized set of
643 variables since vegetation heterogeneity and other site level characteristics can influence
644 ecosystem ET levels (Eichelmann et al., 2018).

645 This is also evident in the validation using data from the winter/senescent period,
646 where F11 performed best at Mayberry Farms and Sherman Island, whereas F36 performed
647 best at East End and West Pond. The overall performance of our ANNs in predicting E
648 during the winter/senescent periods was also considerably lower in comparison to the
649 flooding and leaf-level data validation. This is partially due to the smaller fluxes observed
650 overall during this period, leading to larger relative errors. In addition, the assumption that all
651 measured ET during the winter months represents solely E is likely incorrect. Especially at
652 the sites with high vegetation cover (Mayberry and West Pond) it is likely that a small
653 amount of T occurs during this time which would be included in the measured ET signal,
654 leading to an apparent under-prediction of E for the ANN. For East End and Sherman Island,
655 however, we can see that the ANNs are actually over-predicting E (Fig. 2), leading to
656 consistent, albeit relatively small, negative T prediction in the winter months, specifically at
657 East End (Fig. 4). It is unclear what is causing the discrepancy between measured and
658 modeled E at East End and Sherman Island during the winter months. However, the fact that
659 inclusion of variables linked to vegetation growth (GCC, wc_gf, er_Reichstein) reduced the
660 over-prediction at both sites (e.g., F36 or F15) could indicate that E dynamics linked to
661 phenology and vegetation cover are not adequately reproduced in models without these input
662 variables at East End and Sherman Island.

663 Unfortunately, a limitation in our study is that we were not able to validate our
664 results across all sites/sampling times due to a lack of leaf-level data collected from all sites,
665 which is very time and labor intensive. In addition, no data were available from the initial
666 flooding period at the West Pond wetland. Nonetheless, we are aware that validation of T/ET
667 partitioning is quite scarce in the literature and that the data validated against our ANNs
668 prove that good results can be achieved using the protocol tested here.

669

670 **4.3 Artificial Neural Network Performance Across the Wetland Sites**

671

672 Concerning the performance of all the 36 ANNs across the four wetlands analyzed
673 in this study, West Pond showed smaller testing R^2 values in comparison to the three other
674 sites. Between-site differences reached up to 46% for the same model. The main reason for
675 this divergence was likely the differing amounts of open water surfaces and density of the
676 vegetation between these sites. West Pond, with little to no open water, is likely to see less E
677 compared to the other wetlands (Eichelmann et al., 2018). In addition, West Pond also has the
678 lowest water temperature and a very dense vegetation canopy decoupling the water surface
679 from the atmosphere and leading to further reductions in E, especially at night (Drexler et al.,
680 2004; Goulden et al., 2007; Eichelmann et al., 2018). Because our method predicts E based
681 on nighttime data and calculates T based on the difference between total ET and E, if E
682 values are small the relative accuracy of the prediction will decrease, which is reflected in the
683 testing R^2 values. However, because the E values are small, the absolute error of the predicted
684 E and T would be proportionately small, hence the total T and E values can still be reliable.
685 Unfortunately, we did not have a set of ground-truth validation data available for the West
686 Pond site to investigate the true performance of the ANN ET partitioning. However, our
687 comparison with the Scott and Biederman (2017) partitioned data and expected relationships
688 based on the observed carbon fluxes and vegetation dynamics give us high confidence in the

689 performance of the ANN partitioning routine at the West Pond wetland site. This shows that
690 the ANN partitioning method can also be successfully applied in situations where nighttime E
691 fluxes are small, indicating that it could be applicable to a large variety of ecosystems.

692

693 **4.4 Comparisons with Other Partitioning Approaches**

694

695 In comparison to other established methods in the literature our own approach using
696 ANNs to determine the T/ET partitioning achieved very good results with fewer limitations,
697 which makes it easier to apply in other contexts/ecosystems. For instance, Scott and
698 Biederman's (2017) method only works when there are enough years of data. The shortest
699 dataset Scott and Biederman (2017) analyzed spanned eight years, which is a considerably
700 long time period and reduces its applicability to shorter studies. Also, in the absence of
701 climate consistency among sampling sites or if the research takes place in areas where fluxes
702 are not limited by water availability (e.g., wetlands), their model fails to partition T/ET
703 correctly, limiting it to relatively dry ecosystems. This was evident from direct comparisons
704 with our own method, particularly for Sherman Island which has the shortest dataset (i.e.,
705 four years) and the highest area of open water, with the largest relative contribution of E (Fig.
706 4, 5).

707 Considering the partitioning methods proposed by Scanlon and Sahu (2008),
708 Scanlon and Kustas (2010), and Skaggs et al. (2018), a priori knowledge on WUE and carbon
709 uptake is required to apply their method. Consequently, the paucity of previous
710 data/information or lack of equipment impede the application of this method to a broader
711 audience. We tried to run the Scanlon and Kustas (2010) and Skaggs et al. (2018) partitioning
712 methods for our wetland sites but were not able to retrieve reliable and meaningful
713 partitioning results for any of the sites discussed in this study. We did not test the method
714 proposed by Zhou et al. (2016) in this study, since we believe that some of the underlying

715 assumptions are easily violated at the wetland sites investigated here. Most importantly, the
716 Zhou et al. (2016) method is based on the assumption that some periods within the time series
717 represent conditions without E and the water flux is entirely based on T (i.e., $T = ET$). This is
718 most certainly not the case at flooded sites where we can reasonably expect that there will
719 always be E, albeit in varying amounts. Additionally, the potential underlying WUE is
720 assumed to be constant, which could be violated when multiple vegetation types or species
721 are present, as is the case with our sites. Finally, virtually all the other methods discussed
722 here lacked validation against ground-truth data in the original studies. We included several
723 verification types for the ANN method in this paper, which gives us confidence that our
724 approach using ANNs produces reliable and meaningful estimates for E and T in wetland
725 ecosystems. The fact that our method does not rely on presumed relationships between water
726 and carbon fluxes and was shown to work across a range of ecosystem properties from T to E
727 dominated systems, provides an advantage against other methods that are limited to certain
728 ecosystems or need specialized input data/equipment.

729

730 **5 Summary**

731

732 A novel T/ET partitioning method using Artificial Neural Networks (ANN) to
733 predict daytime E from nighttime ET measurements in a combination with a range of
734 environmental variables was presented and compared to previous methods from the literature.
735 In comparison to other approaches, the ANN method achieved better results, particularly with
736 shorter-term data (i.e., <5 years) and was successfully applied to flooded ecosystems. The
737 order of variable inclusion (and importance) for the ANN construction was: vapor pressure
738 deficit (VPD) > gap-filled sensible heat flux (H_{gf}) > air temperature (T_{air}) > friction velocity
739 (u_*) > other variables. The best performing ANN, model F11, used datetime, VPD, H_{gf} , T_{air} ,
740 and u_* inputs with an average testing R^2 value across all sites of 0.85. This model also

741 performed the best when validated against ground-truth leaf-level data and periods where
742 sites were completely flooded with no T from vegetation. Our method sheds light on T/ET
743 partitioning methods and applications. While here it has only been tested for flooded
744 ecosystems, we present strong indicators that it could also perform well in other ecosystems,
745 contributing to the understanding of the global water cycle.

746

747 **6 Acknowledgments**

748 **Author contributions:** Conceptualization: E.E., D.D.B.; Data collection and
749 processing: E.E., S.D.C., K.S.H., P.Y.O., D.S., A.V., J.V.; Formal analysis: E.E.; M.C.M;
750 Writing—original draft: E.E., M.C.M; Writing—review and editing: D.D.B., A.V., K.S.H.,
751 P.Y.O.;

752 **Funding sources:** This work was supported by Enterprise Ireland (H2020- Proposal
753 Preparation Support CS20202080); the California Department of Water Resources (DWR)
754 through a contract from the California Department of Fish and Wildlife; and the United States
755 Department of Agriculture (NIFA grant #2011-67003-30371). Funding for the AmeriFlux
756 core sites was provided by the U.S. Department of Energy's Office of Science (AmeriFlux
757 contract #7079856). Dennis D. Baldocchi was supported by the McIntire-Stennis Capacity
758 Grant funding to the California Agricultural Experiment Station. Kyle S. Hemes was
759 supported by the California Sea Grant Delta Science Fellowship. This material is based upon
760 work supported by the Delta Stewardship Council Delta Science Program under Grant No.
761 2271 and California Sea Grant College Program Project R/SF-70.

762 **References**

- 764 Baldocchi, D. and Sturtevant, C. (2015). Does day and night sampling reduce spurious
765 correlation between canopy photosynthesis and ecosystem respiration? *Agricultural*
766 *and Forest Meteorology*, 207.
- 767 Baldocchi, D. D. (2003). Assessing the eddy covariance technique for evaluating carbon
768 dioxide exchange rates of ecosystems: past, present and future. *Global Change Biology*,
769 9(4):479–492.
- 770 Baldocchi, D. D., Hicks, B. B., and Meyers, T. P. (1988). Measuring biosphere-atmosphere
771 exchanges of biologically related gases with micrometeorological methods. *Ecology*,
772 69(5):1331–1340.
- 773 Barr, A. G., Black, T. A., Hogg, E. H., Kljun, N., Morgenstern, K., and Nesic, Z. (2004).
774 Inter-annual variability in the leaf area index of a boreal aspen-hazelnut forest in
775 relation to net ecosystem production. *Agricultural and Forest Meteorology*, 126(3-
776 4):237–255.
- 777 Brutsaert, W. and Parlange, M. B. (1998). Hydrologic cycle explains the evaporation
778 paradox. *Nature*, 396(6706):30.
- 779 Buckley, T. N. (2005). The Control of Stomata by Water Balance. *The New Phytologist*,
780 168(2):275–291.
- 781 Caird, M. A., Richards, J. H., and Donovan, L. A. (2006). Nighttime Stomatal Conductance
782 and Transpiration in C3 and C4 Plants. *Plant Physiology*, 143(1):4–10.
- 783 Chamberlain, S. D., Hemes, K. S., Eichelmann, E., Szutu, D. J., Verfaillie, J. G., &
784 Baldocchi, D. D. (2020). Effect of Drought-Induced Salinization on Wetland Methane
785 Emissions, Gross Ecosystem Productivity, and Their Interactions. *Ecosystems*, 23(3),
786 675–688.

- 787 Dawson, T. E., Burgess, S. S., Tu, K. P., Oliveira, R. S., Santiago, L. S., Fisher, J. B.,
788 Simonin, K. A., and Ambrose, A. R. (2007). Nighttime transpiration in woody plants
789 from contrasting ecosystems. *Tree Physiology*, 27(4):561–575.
- 790 Desai, A. R., Richardson, A. D., Moffat, A. M., Kattge, J., Hollinger, D. Y., Barr, A., Falge,
791 E., Noormets, A., Papale, D., Reichstein, M., and Stauch, V. J. (2008). Cross-site
792 evaluation of eddy covariance GPP and RE decomposition techniques. *Agricultural
793 and Forest Meteorology*, 148(6-7):821–838.
- 794 Detto, M., Baldocchi, D., and Katul, G. G. (2010). Scaling Properties of Biologically Active
795 Scalar Concentration Fluctuations in the Atmospheric Surface Layer over a Managed
796 Peatland. *Boundary-Layer Meteorology*, 136(3):407–430.
- 797 Deverel, S. J. and Rojstaczer, S. (1996). Subsidence of agricultural lands in the Sacramento-
798 San Joaquin Delta, California: Role of aqueous and gaseous carbon fluxes. *Water
799 Resources Research*, 32(8):2359–2367.
- 800 Drexler, J. Z., Snyder, R. L., Spano, D., and Paw U, K. T. (2004). A review of models and
801 micrometeorological methods used to estimate wetland evapotranspiration.
802 *Hydrological Processes*, 18(11):2071–2101.
- 803 Dronova, I. and Taddeo, S. (2016). Canopy Leaf Area Index in Non-Forested Marshes of the
804 California Delta. *Wetlands*, 36(4):705–716.
- 805 Eichelmann, E., Hemes, K. S., Knox, S. H., Oikawa, P. Y., Chamberlain, S. D., Sturtevant,
806 C., Verfaillie, J., and Baldocchi, D. D. (2018). The effect of land cover type and
807 structure on evapotranspiration from agricultural and wetland sites in the Sacramento-
808 San Joaquin River Delta, California. *Agricultural and Forest Meteorology*, 256-
809 257:179–195.
- 810 Foken, T. and Wichura, B. (1996). Tools for quality assessment of surface-based flux
811 measurements. *Agricultural and Forest Meteorology*, 78(1-2):83–105.

- 812 Gerken, T., Bromley, G. T., and Stoy, P. C. (2018). Surface moistening trends in the Northern
813 North American great plains increase the likelihood of convective initiation. *Journal of*
814 *Hydrometeorology*, 19(1):227–244.
- 815 Goulden, M. L., Litvak, M., and Miller, S. D. (2007). Factors that control Typha marsh
816 evapotranspiration. *Aquatic Botany*, 86(2):97–106.
- 817 Hatala, J. A., Detto, M., Sonnentag, O., Deverel, S. J., Verfaillie, J., and Baldocchi, D. D.
818 (2012). Greenhouse gas (CO₂, CH₄, H₂O) fluxes from drained and flooded agricultural
819 peatlands in the Sacramento-San Joaquin Delta. *Agriculture, Ecosystems &*
820 *Environment*, 150:1–18.
- 821 Hemes, K. S., Chamberlain, S. D., Eichelmann, E., Anthony, T., Valach, A., Kasak, K.,
822 Szutu, D., Verfaillie, J., Silver, W. L., and Baldocchi, D. D. (2019). Assessing the
823 carbon and climate benefit of restoring degraded agricultural peat soils to managed
824 wetlands. *Agricultural and Forest Meteorology*, 268:202–214.
- 825 Hemes, K. S., Eichelmann, E., Chamberlain, S., Knox, S. H., Oikawa, P. Y., Sturtevant, C.,
826 Verfaillie, J., Szutu, D., and Baldocchi, D. D. (2018). A unique combination of
827 aerodynamic and surface properties contribute to surface cooling in restored wetlands
828 of the Sacramento-San Joaquin Delta, California. *Journal of Geophysical Research:*
829 *Biogeosciences*, 123(7):2072–2090.
- 830 Jung, M., Koirala, S., Weber, U., Ichii, K., Gans, F., Gustau-Camps-Valls, Papale, D.,
831 Schwalm, C., Tramontana, G., and Reichstein, M. (2018). The FLUXCOM ensemble of
832 global land-atmosphere energy fluxes. arXiv:1812.04951 [physics.ao-ph]
- 833 Knox, S. H., Matthes, J. H., Sturtevant, C., Oikawa, P. Y., Verfaillie, J., and Baldocchi, D. D.
834 (2016). Biophysical controls on interannual variability in ecosystem scale CO₂ and
835 CH₄ exchange in a California rice paddy. *Journal of Geophysical Research:*
836 *Biogeosciences*, 121(3):978–1001.

- 837 Knox, S. H., Sturtevant, C., Matthes, J. H., Koteen, L., Verfaillie, J., and Baldocchi, D.
838 (2015). Agricultural peatland restoration: effects of land-use change on greenhouse gas
839 (CO₂ and CH₄) fluxes in the Sacramento-San Joaquin Delta. *Global Change Biology*,
840 21(2):750–65.
- 841 Li, X., Gentine, P., Lin, C., Zhou, S., Sun, Z., Zheng, Y., Liu, J., and Zheng, C. (2019). A
842 simple and objective method to partition evapotranspiration into transpiration and
843 evaporation at eddy-covariance sites. *Agricultural and Forest Meteorology*, 265:171–
844 182.
- 845 Miralles, D. G., Brutsaert, W., Dolman, A. J., and Gash, J. H. (2020). On the Use of the Term
846 “Evapotranspiration”. *Water Resources Research*, 56(11):e2020WR028055.
- 847 Moffat, A. M., Papale, D., Reichstein, M., Hollinger, D. Y., Richardson, A. D., Barr, A. G.,
848 Beckstein, C., Braswell, B. H., Churkina, G., Desai, A. R., Falge, E., Gove, J. H.,
849 Heimann, M., Hui, D., Jarvis, A. J., Kattge, J., Noormets, A., and Stauch, V. J. (2007).
850 Comprehensive comparison of gap-filling techniques for eddy covariance net carbon
851 fluxes. *Agricultural and Forest Meteorology*, 147(3-4):209–232.
- 852 Nelson, J. A., Carvalhais, N., Cuntz, M., Delpierre, N., Knauer, J., Ogée, J., Migliavacca, M.,
853 Reichstein, M., and Jung, M. (2018). Coupling Water and Carbon Fluxes to Constrain
854 Estimates of Transpiration: The TEA Algorithm. *Journal of Geophysical Research:*
855 *Biogeosciences*, 123(12):3617–3632.
- 856 Novick, K. A., Ficklin, D. L., Stoy, P. C., Williams, C. A., Bohrer, G., Oishi, A., Papuga, S.
857 A., Blanken, P. D., Noormets, A., Sulman, B. N., Scott, R. L., Wang, L., and Phillips,
858 R. P. (2016). The increasing importance of atmospheric demand for ecosystem water
859 and carbon fluxes. *Nature Climate Change*, 6(11):1023–1027.
- 860 O’Connell, J. L., Byrd, K. B., Kelly, M., Gould, R. W., Inoue, Y., and Thenkabail, P. S.
861 (2015). A Hybrid Model for Mapping Relative Differences in Belowground Biomass

- 862 and Root:Shoot Ratios Using Spectral Reflectance, Foliar N and Plant Biophysical Data
863 within Coastal Marsh. *Remote Sensing*, 7:16480–16503.
- 864 Oikawa, P. Y., Sturtevant, C., Knox, S. H., Verfaillie, J., Huang, Y. W., and Baldocchi, D. D.
865 (2017). Revisiting the partitioning of net ecosystem exchange of CO₂ into
866 photosynthesis and respiration with simultaneous flux measurements of ¹³CO₂ and
867 CO₂, soil respiration and a biophysical model, CANVEG. *Agricultural and Forest
868 Meteorology*, 234-235:149–163.
- 869 Oki, T. and Kanae, S. (2006). Global Hydrological Cycles and World Water Resources.
870 *Science*, 313(5790):1068 LP – 1072.
- 871 Papale, D. and Valentini, R. (2003). A new assessment of European forests carbon exchanges
872 by eddy fluxes and artificial neural network spatialization. *Global Change Biology*,
873 9(4):525–535.
- 874 Reichstein, M., Falge, E., Baldocchi, D., Papale, D., Aubinet, M., Berbigier, P., Bernhofer,
875 C., Buchmann, N., Gilmanov, T., Granier, A., Grunwald, T., Havrankova, K.,
876 Ilvesniemi, H., Janous, D., Knohl, A., Laurila, T., Lohila, A., Loustau, D., Matteucci,
877 G., Meyers, T., Miglietta, F., Ourcival, J.-M., Pumpanen, J., Rambal, S., Rotenberg, E.,
878 Sanz, M., Tenhunen, J., Seufert, G., Vaccari, F., Vesala, T., Yakir, D., and Valentini, R.
879 (2005). On the separation of net ecosystem exchange into assimilation and ecosystem
880 respiration: review and improved algorithm. *Global Change Biology*, 11(9):1424–1439.
- 881 Scanlon, T. M. and Kustas, W. P. (2010). Partitioning carbon dioxide and water vapor fluxes
882 using correlation analysis. *Agricultural and Forest Meteorology*, 150(1):89–99.
- 883 Scanlon, T. M. and Sahu, P. (2008). On the correlation structure of water vapor and carbon
884 dioxide in the atmospheric surface layer: A basis for flux partitioning. *Water Resources
885 Research*, 44(10).
- 886 Schlesinger, W. H. and Jasechko, S. (2014). Transpiration in the global water cycle.
887 *Agricultural and Forest Meteorology*, 189-190:115–117.

- 888 Schmidt, A., Hanson, C., Chan, W. S., and Law, B. E. (2012). Empirical assessment of
889 uncertainties of meteorological parameters and turbulent fluxes in the AmeriFlux
890 network. *Journal of Geophysical Research: Biogeosciences*, 117(G4):0148-0227.
- 891 Scott, R. L. and Biederman, J. A. (2017). Partitioning evapotranspiration using long-term
892 carbon dioxide and water vapor fluxes. *Geophysical Research Letters*, 44(13):6833–
893 6840.
- 894 Skaggs, T., Anderson, R., Alfieri, J., Scanlon, T., and Kustas, W. (2018). Fluxpart: Open
895 source software for partitioning carbon dioxide and water vapor fluxes. *Agricultural
896 and Forest Meteorology*, 253-254:218–224.
- 897 Stoy, P. C., El-Madany, T., Fisher, J. B., Gentine, P., Gerken, T., Good, S. P., Liu, S.,
898 Miralles, D. G., Perez-Priego, O., Skaggs, T. H., Wohlfahrt, G., Anderson, R. G., Jung,
899 M., Maes, W. H., Mammarella, I., Mauder, M., Migliavacca, M., Nelson, J. A.,
900 Poyatos, R., Reichstein, M., Scott, R. L., and Wolf, S. (2019). Reviews and syntheses:
901 Turning the challenges of partitioning ecosystem evaporation and transpiration into
902 opportunities. *Biogeosciences Discussions*, pages 1–47.
- 903 Tramontana, G., Migliavacca, M., Jung, M., Reichstein, M., Keenan, T. F., Camps-Valls, G.,
904 Ogee, J., Verrelst, J., and Papale, D. (2020). Partitioning net carbon dioxide fluxes into
905 photosynthesis and respiration using neural networks. *Global Change Biology*,
906 26(9):5235–5253.
- 907 Trenberth, K. E., Fasullo, J. T., and Kiehl, J. (2009). Earth’s Global Energy Budget. *Bulletin
908 of the American Meteorological Society*, 90(3):311–324.
- 909 Valach, A.C., Kasak., K., Hemes, K., Anthony, T., Taddeo, S., Dronova, I., Silver, W., Szutu,
910 D., Verfaillie, J., Baldocchi, D. (2021). Productive wetlands restored for carbon
911 sequestration quickly become net CO₂ sinks with site-level factors driving uptake
912 variability, *PLOS One*, 16(3): e0248398.

- 913 Webb, E. K., Pearman, G. I., and Leuning, R. (1980). Correction of flux measurements for
914 density effects due to heat and water vapour transfer. *Quarterly Journal of the Royal*
915 *Meteorological Society*, 106(447):85–100.
- 916 Wilson, K., Goldstein, A., Falge, E., Aubinet, M., Baldocchi, D. D., Berbigier, P., Bernhofer,
917 C., Ceulemans, R., Dolman, H., Field, C., Grelle, A., Ibrom, A., Law, B. E., Kowalski,
918 A., Meyers, T. P., Moncrieff, J., Monson, R., Oechel, W., Tenhunen, J., Valentini, R.,
919 and Verma, S. (2002). Energy balance closure at FLUXNET sites. *Agricultural and*
920 *Forest Meteorology*, 113(1-4):223–243.
- 921 Wilson, K. B., Hanson, P. J., Mulholland, P. J., Baldocchi, D. D., and Wullschleger, S. D.
922 (2001). A comparison of methods for determining forest evapotranspiration and its
923 components: sap-flow, soil water budget, eddy covariance and catchment water
924 balance. *Agricultural and Forest Meteorology*, 106(2):153–168.
- 925 Zeng, Z., Piao, S., Li, L. Z. X., Wang, T., Ciais, P., Xu, L., Yang, Y., Mao, J., Shi, X., and
926 Myneni, R. B. (2018). Impact of Earth Greening on the Terrestrial Water Cycle.
927 *Journal of Climate*, 31(7):2633–2650.
- 928 Zhou, S., Yu, B., Zhang, Y., Huang, Y., and Wang, G. (2016). Partitioning evapotranspiration
929 based on the concept of underlying water use efficiency. *Water Resources Research*,
930 52(2):1160–1175.
- 931

932 **Table 1:** Average testing R^2 and slope values for 12 ANN architecture models used to
 933 partition evapotranspiration measurements, demonstrating an increase in complexity from
 934 models F21 (most basic) to F36 (most complex).

Model Name	Model Structure	Average testing R^2	Average Slope
F21	datetime	0.410	0.393
F26	datetime + VPD	0.648	0.626
F17	datetime + VPD + T_{air}	0.672	0.636
F31	datetime + VPD + T_{air} + GCC	0.686	0.657
F32	datetime + VPD + T_{air} + GCC + Rnet	0.689	0.665
F15	datetime + VPD + T_{air} + GCC + Rnet + WT	0.694	0.663
F33	datetime + H_{gf} + VPD	0.753	0.726
F34	datetime + H_{gf} + VPD + T_{air}	0.762	0.734
F11	datetime + H_{gf} + VPD + T_{air} + u_*	0.853	0.831
F35	datetime + H_{gf} + VPD + T_{air} + u_* + er_Reichstein	0.863	0.851
F14	datetime + H_{gf} + u_* + VPD + T_{air} + GCC + Rnet + WT	0.877	0.868
F36	datetime + H_{gf} + u_* + wc_{gf} + er_Reichstein + VPD + T_{air} + GCC + Rnet + WT	0.891	0.880

935

936

937 **Table 2:** Validation R^2 and slope values of seven ANNs used to partition evapotranspiration
938 measurements and validated with data collected right after flooding for East End, Mayberry
939 Farms, and Sherman Island wetland sites. Models are ordered by the increase in complexity,
940 from model F21 (most basic) to F36 (most complex). Refer to Tables 1 and 3 for each
941 model's input variables. Validation R^2 values higher than 0.7 are highlighted in bold.

Model Name	East End		Mayberry Farms		Sherman Island	
	R^2	Slope	R^2	Slope	R^2	Slope
F21	0.29	0.28	0.06	0.09	0.34	0.25
F26	0.48	0.52	0.26	0.37	0.61	0.50
F17	0.50	0.46	0.31	0.41	0.63	0.56
F15	0.24	0.15	0.16	0.13	0.37	0.28
F33	0.61	0.66	0.48	0.81	0.62	0.71
F11	0.81	0.86	0.69	0.95	0.82	1.00
F36	0.51	0.45	0.56	0.48	0.53	0.43

942

943

944 **Table 3:** Validation R^2 and slope values of seven ANNs used to partition evapotranspiration
945 measurements and validated with winter time data (December to February) for each of the
946 four wetlands studied (East End, Mayberry Farms, Sherman Island, and West Pond). Models
947 are listed according to the increase in complexity, from model F21 (most basic) to F36 (most
948 complex). Refer to Tables 1 and 4 for each model's input variables. Validation R^2 values
949 higher than 0.7 are highlighted in bold.

Model Name	East End		Mayberry Farms		Sherman Island		West Pond	
	R^2	Slope	R^2	Slope	R^2	Slope	R^2	Slope
F21	0.06	0.02	0.06	0.06	0.15	0.11	0.08	0.30
F26	0.17	0.25	0.26	0.38	0.45	0.48	0.03	0.08
F17	0.21	0.24	0.35	0.47	0.47	0.49	0.05	0.06
F15	0.33	0.41	0.14	0.12	0.43	0.29	0.17	0.11
F33	0.21	0.71	0.22	0.48	0.19	0.42	0.01	0.01
F11	0.33	1.15	0.56	0.71	0.70	1.27	0.11	0.11
F36	0.45	0.95	0.43	0.59	0.69	0.87	0.36	0.17

950

951

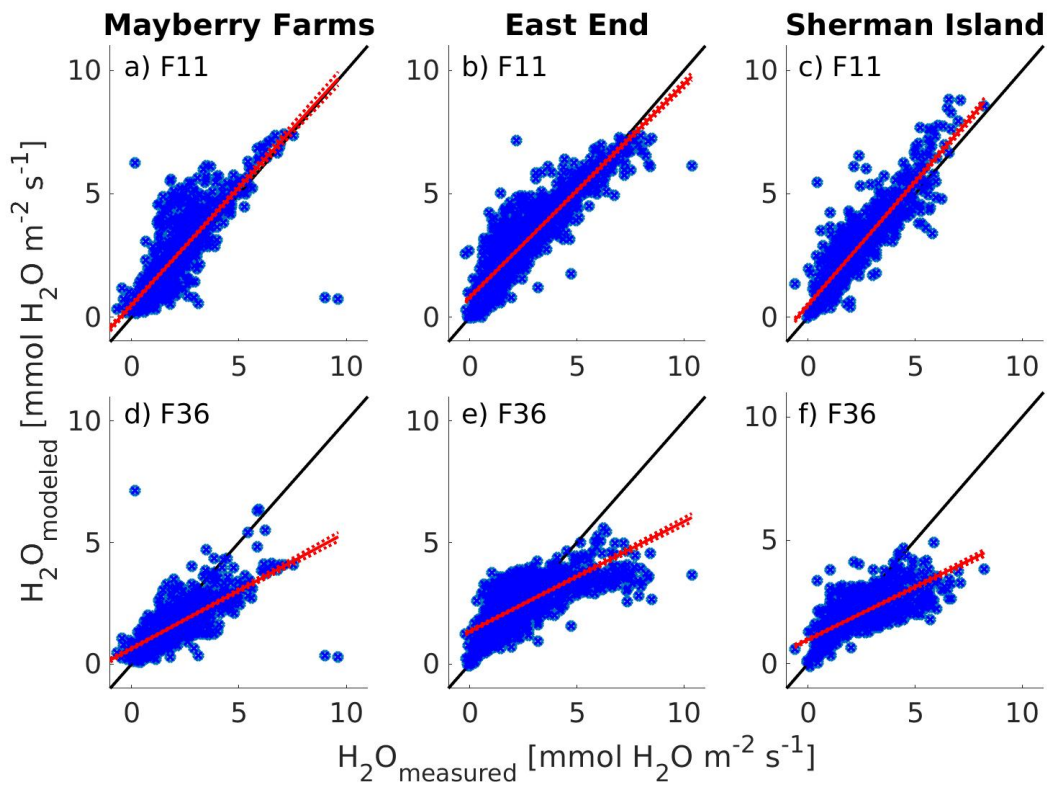
952 **Table 4:** R² and slope values for linear regression of ecosystem level transpiration data
953 predicted by seven ANNs versus leaf-level transpiration data collected in 2017 for East End.
954 Models are ordered by the increase in complexity from model F21 (most basic) to F36 (most
955 complex).

Model Name	Model Structure	R² value	Slope value
F21	datetime	0.979	0.95
F26	datetime + VPD	0.984	0.79
F17	datetime + VPD + TA	0.984	0.75
F15	datetime + VPD + TA + GCC + Rnet + WT	0.987	0.81
F33	datetime + H_gf + VPD	0.99	0.93
F11	datetime + H_gf + VPD + TA + u _*	0.986	0.76
F36	datetime + H_gf + u _* + wc_gf + er_Reichstein + VPD + TA + GCC + Rnet + WT	0.922	0.70

956

957

958

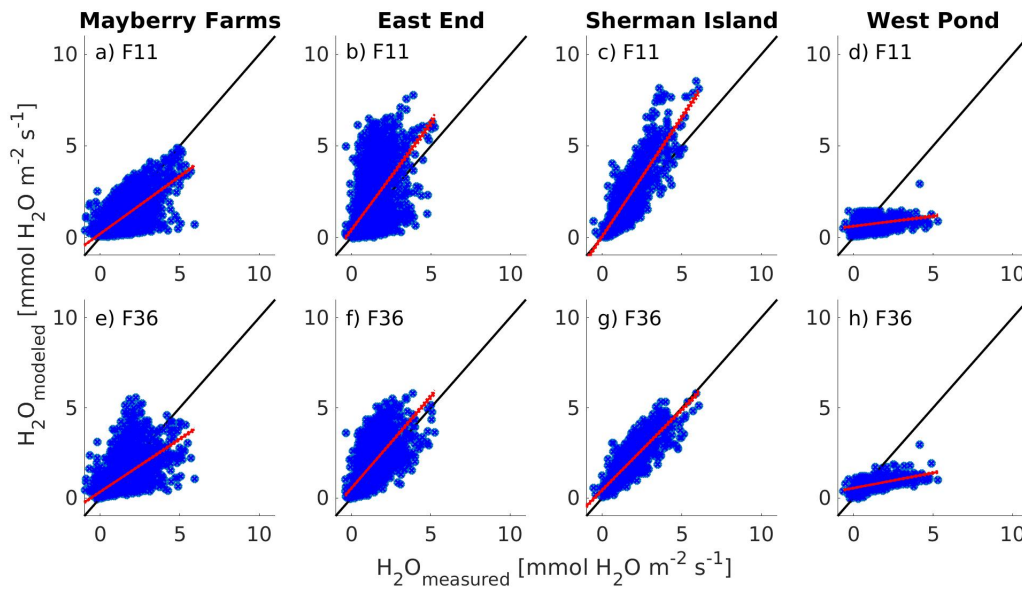


959

960 **Figure 1:** Comparison between the eddy covariance measured daytime evaporation flux
961 ($H_{2}O_{\text{measured}}$) and daytime evaporation predicted by ANNs ($H_{2}O_{\text{modeled}}$) using model F11 (top
962 panels, a-c) and F36 (bottom panels, d-f) based on data collected right after flooding for
963 Mayberry Farms (a, d), East End (b, e), and Sherman Island (c, f). Note: the black lines are
964 1:1 relationships for reference, red lines show linear regressions with standard deviation, and
965 blue dots represent the data.

966

967

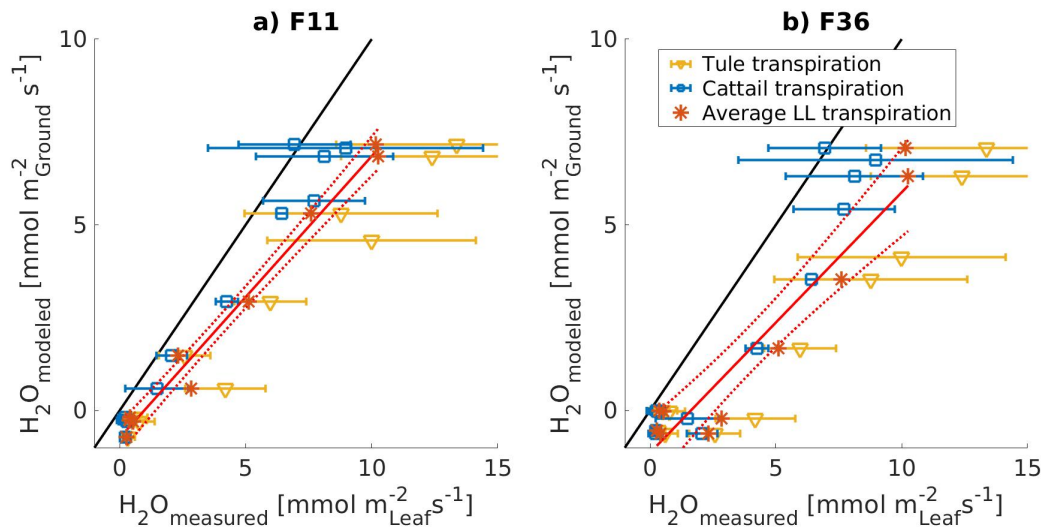


968

969 **Figure 2:** Comparison between the eddy covariance measured daytime evaporation flux
970 ($H_{2}O_{\text{measured}}$) and daytime evaporation predicted by ANNs ($H_{2}O_{\text{modeled}}$) using model F11 (top
971 panels, a-d) and F36 (bottom panels, e-h) based on data collected during senescent periods in
972 winter (December to February) at Mayberry Farms (a, e), East End (b, f), Sherman Island (c,
973 g), and West Pond (d, h). Note: the black lines are 1:1 relationships for reference, red lines
974 show linear regressions with standard deviation, and blue dots represent the data.

975

976



977

978 **Figure 3:** Ecosystem level transpiration data (H_2O_{modeled}) predicted by ANNs F11 (a) and F36

979 (b) validated against leaf-level transpiration data (H_2O_{measured}) collected during the field

980 campaigns in 2017 for the two dominant species in the wetland: Tule (yellow triangles) and

981 Cattail (blue squares). The overall linear regression line (solid red line) and standard

982 deviation (dashed red line) is based on average leaf-level transpiration across both species

983 (red asterisks). Error bars represent the standard deviation from the mean for each

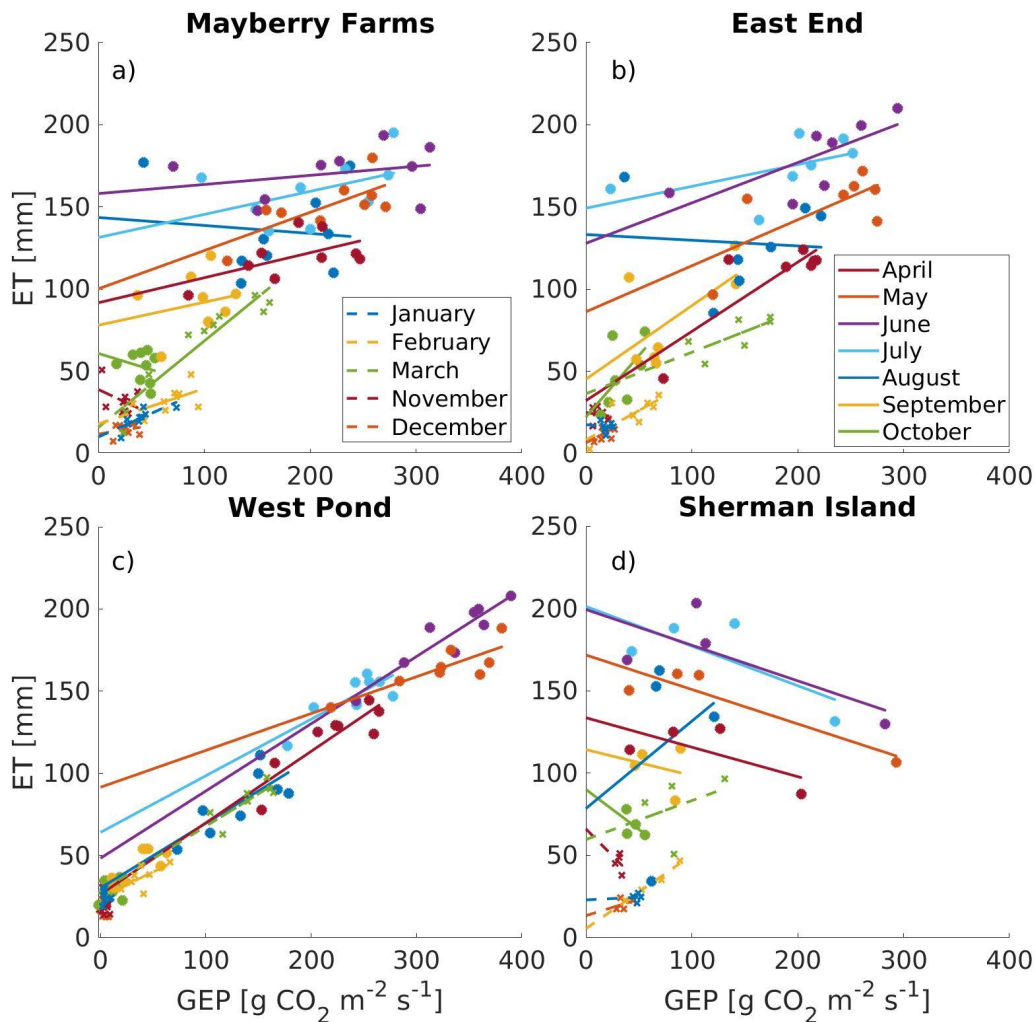
984 measurement interval and species for the leaf-level data. Leaf-level data were pooled for 30

985 min intervals to match the eddy covariance averaging period. The solid black lines show 1:1

986 relationships for reference.

987

988

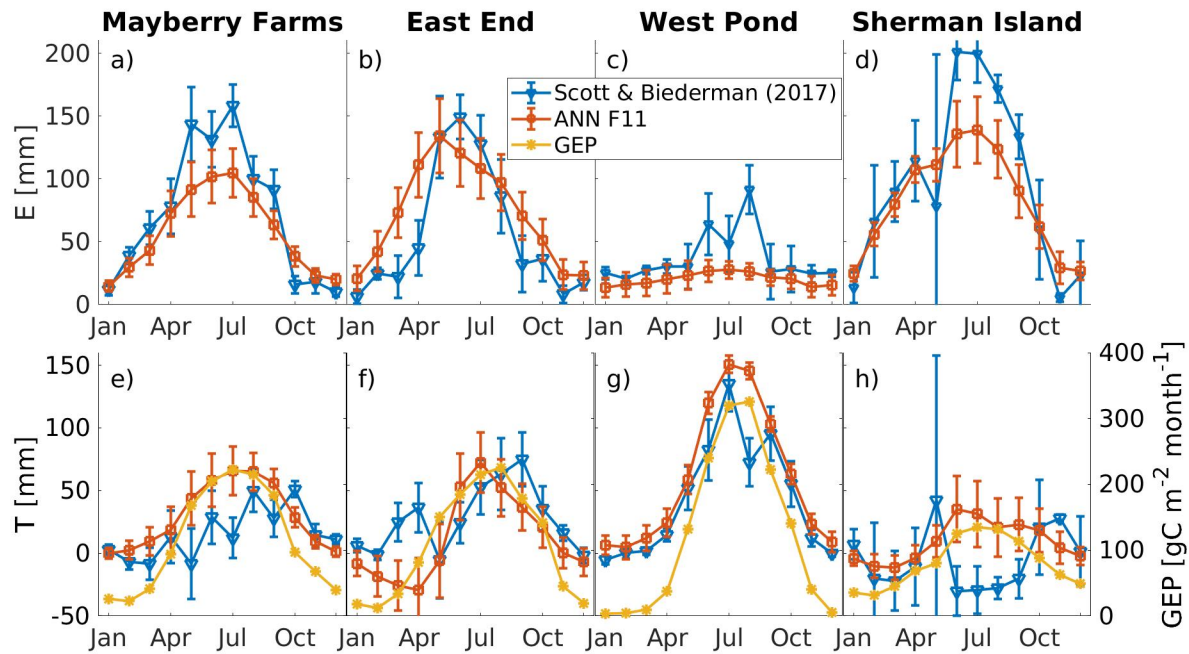


989

990 **Figure 4:** Monthly regressions of evapotranspiration (ET) vs Gross Ecosystem Productivity
991 (GEP) data for four wetland sites Mayberry Farms (a), East End (b), West Pond (c), and
992 Sherman Island (d) for T/ET partitioning using the Scott and Biederman (2017) method for
993 long-term flux data. Each regression line represents data for the same month across multiple
994 years. The method is considered unreliable for winter months when GEP is small (November
995 through March, shown in dashed lines and cross symbols). Negative regression lines for most
996 months at Sherman Island (d) indicate that the methodology does not work at this site,
997 potentially due to the shorter time period of this dataset (4 years) or because of the large
998 contribution of evaporation at this site (see main text for detailed discussion).

999

1000



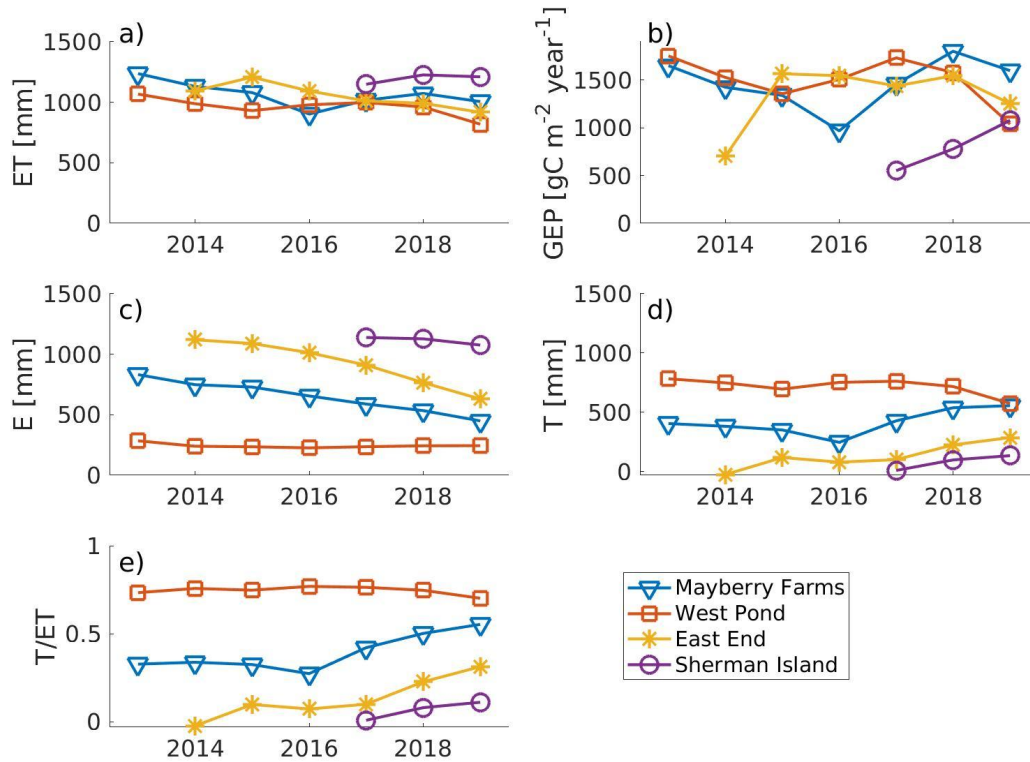
1001

1002 **Figure 5:** Average monthly evaporation (E) (top panels, a-d) and transpiration (T) (bottom
1003 panels, e-h) fluxes across four wetland sites: Mayberry Farms (a, e), East End (b, f), West
1004 Pond (c, g), and Sherman Island (d, h) comparing the ANN T/ET partitioning method
1005 described in this paper (red lines and square symbols) and the Scott and Biederman (2017)
1006 method (blue lines and triangle symbols) on long-term flux data. Error bars are based on the
1007 standard error of the fit intercept and slope for the Scott and Biederman (2017) method and
1008 on the interquartile range of the 20 individual ANN runs for the ANN method. Comparisons
1009 were done using ANN F11 for all sites. Gross Ecosystem Productivity (GEP, yellow lines and
1010 asterisks) for each site is shown for comparison in the bottom panels with a separate y-axis on
1011 the right.

1012

1013

1014



1015

1016 **Figure 6:** Annual intercomparison of (a) total evapotranspiration (ET), (b) gross ecosystem
1017 productivity (GEP), (c) evaporation (E), (d) transpiration (T), and (e) transpiration over
1018 evapotranspiration ratio (T/ET) between four wetland sites (Mayberry Farms, 2013-2019,
1019 blue triangles; West Pond, 2013-2019, red squares; East End, 2014-2019, yellow asterisks;
1020 and Sherman Island, 2016-2019, purple circles). E and T values are based on the ANN
1021 partitioning routine (F11) described in this study.

1022

1023